Geochemical Perspectives Letters

Hafnium isotopes in zircons document the gradual onset of mobile-lid tectonics

A.M. Bauer and J.R. Reimink, T. Chacko, B.J. Foley, S.B. Shirey, D.G. Pearson

Supplementary Information

The Supplementary Information includes:

- Supplementary Discussion
- Figures S-1 to S-12
- Supplementary Information References

Supplementary Discussion

Restricted sourcing of detrital zircons in Archean cover group sequences

Our hypothesis of a global shift in tectonic regime relies on the globally representative nature of the compilation of detrital zircon suites that we have considered. In this section, we show that the current understanding of the sedimentary sequences containing ancient detrital zircons indicates restricted sourcing and small catchment size, which in turn strongly suggests that the detrital zircon suites considered here were derived from different terranes rather than sourced in a single, ancient terrane.

The sedimentary rocks that host Eoarchean-Hadean detrital zircons evaluated here are typically quartzites and conglomerates, which in places are interlayered with banded iron formations (Froude *et al*., 1983; Bleeker *et al*., 1999; Sircombe *et al*., 2001; Thern and Nelson, 2012). Though many of these terranes have only recently been recognised to contain very old zircons, the Jack Hills and Slave craton zircon suites have been studied for decades and can aid in the interpretation of our global compilation. The Jack Hills detrital zircon suite is hosted in the Jack Hills greenstone belt, found along the southern edge of the Narryer Terrane in the Yilgarn Craton. The vast majority of analytical work focused on the Jack Hills detrital zircons has been dedicated to a relatively restricted outcrop (~2 m^2), sample locality W74. A broader analysis of detrital zircons from the Yilgarn Craton (Thern and Nelson, 2012) indicates a substantial amount of regionality in the detrital zircon source terranes from sequence to sequence. Thern and Nelson (2012) concluded that even when considering samples containing >3.9 Ga zircons, distinct source terranes were required to explain the detrital zircon age distributions. Additionally, significant differences exist between the Jack Hills and Acasta Gneiss Complex (AGC) ε_{Hf}-age distributions; in general, the Jack Hills zircons are commonly older and have, on average, lower ε_{Hf} values than Acasta zircons at the same age. Therefore, the Yilgarn detrital zircons were not sourced from the AGC, and instead point to a slightly older crustal precursor.

The AGC is located on the western margin of the Slave craton and is only a small portion of the larger Slave craton basement gneiss assemblage, termed the Central Slave Basement Complex (CSBC; Bleeker *et al*., 1999). Notably, the AGC is the only portion of the broader CSBC that is known to contain >3.4 Ga crust. A thin sedimentary cover group sequence, the Central Slave Cover Group, was deposited directly on top of CSBC and AGC basement rocks between 2.85 and 2.80 Ga (Ketchum *et al*., 2004). This sequence contains detrital zircons that have been analysed for U-Pb (Sircombe *et al*., 2001) and Hf-isotope systematics (Fig. 1c; Pietranik *et al*., 2008). Significant differences in the U-Pb age distributions were documented between distinct locations across the

craton, and Sircombe *et al*. (2001) concluded that the sedimentary input in any one location had a limited diversity, leading to unimodal U-Pb age signatures. Grain size analysis of the detrital zircons substantiated this hypothesis. Whereas Pietranik *et al*. (2008) interpreted the Hf-isotope signatures (collected from the same grains as Sircombe *et al*., 2001) from across the Slave craton as a whole, Reimink *et al*. (2019) focused on regional differences. The latter authors analysed the basement gneiss samples in the core of the Slave craton for their zircon Hf-isotope compositions and found that they had much more positive initial ε_{Hf} values (at the same age) than the concurrent magmatic generations of the AGC (Fig. 1a,c). They compared their basement gneiss samples to the detrital zircon U-Pb-Hf data from the cover group sequences and found that the detrital zircons found in sediments compare well with the basement gneisses directly beneath the sediments (Reimink *et al*. 2019; Fig. S-1). In other words, zircons from any individual sedimentary sample record the age-ε_{Hf} signature of proximal basement gneisses and not the entire craton.

Although most sedimentary packages containing Eoarchean-Hadean detrital zircons have not been studied in great detail, the two locations that have been studied in the most detail (the Yilgarn and Slave cratons) indicate that the sedimentary systems present during this time in Earth history had relatively restricted sedimentary input and localised sources. This conclusion is in line with limited freeboard in the Archean (*e.g*., Flament *et al*., 2008), leading to small basins and restricted sedimentary input. Therefore, it is unlikely that all detrital zircon suites in the current database were sourced from one ancient continental nucleus. The fact that several cratons contain Eoarchean-Hadean detrital zircons with negative initial ε_{Hf} values indicates that these signatures of long protocrustal residence times are representative of global crust formation processes during this time period, and consistent with a stagnant-lid regime.

Summary of the petrology and geochemistry of the Acasta Gneiss Complex

The AGC, which is located on the western margin of the Slave craton, has seen decades of geochronological, geochemical, and petrologic work, with dozens of publications contributing datasets relevant to the interpretations cited in this paper. Several of the authors of the present manuscript recently wrote a review chapter on the AGC that summarises this wealth of data and derives a tectonic model for the formation of the AGC from 4.02–3.4 Ga (Reimink *et al*., 2018b). We point the reader to this chapter for a full discussion of data and references that contributed to the petrologic and tectonic model cited in the present study but summarise key components below.

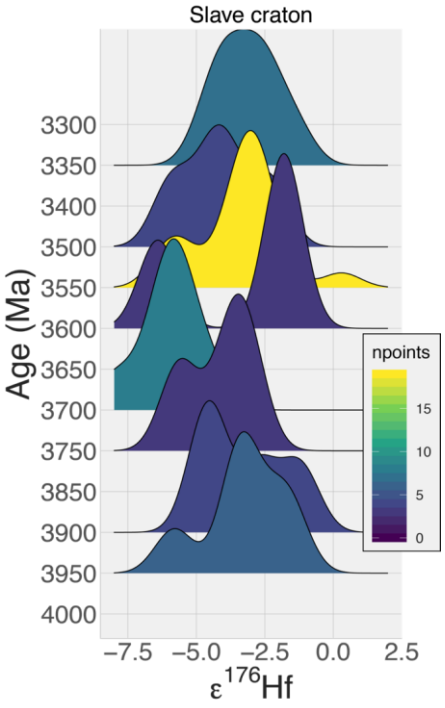

Figure S-1 Stacked probability density estimates for the Slave craton dataset, with the data binned in 50 Myr age bins and plotted separately.

The oldest rocks of the AGC (4.02 Ga) are iron-enriched tonalites with relatively flat REE patterns (low La/Yb) and negative Eu-anomalies. These geochemical signatures suggest formation by shallow-level fractional crystallisation of basaltic magma. Later

AGC magmas (3.96-3.75 Ga) include gabbros and generally more evolved tonalites and granodiorites but share the flat REE patterns and negative Eu anomalies of the oldest rocks. These later magmas formed by relatively shallow-level partial melting of hydrated mafic rocks. Granitoids formed at ~3.6 Ga, when ε_{Hf} values shift from negative to near zero (Fig. 1) and have fundamentally different compositional characteristics—they are more silicic, have steeper REE patterns (high La/Yb), and variable Eu anomalies. The petrological and geochemical characteristics of ~3.6 Ga AGC rocks suggest formation via partial melting of hydrated basalt at great depth, well within the garnet stability field (>40 km). Moreover, the elevated δ18O values of zircon in this suite of AGC granitoids indicate that the magma source rocks had interacted with surface waters before deep burial.

As discussed in the main text, the isotopic record provides strong evidence that AGC rocks older than 3.7 Ga were formed by repeated reworking of Hadean protocrust, whereas < 3.6 Ga rocks require input from a relatively juvenile source. Both the Hf-isotope and ^{142}Nd-isotope systems show this distinct change in magma signatures after 3.6 Ga (Amelin *et al*., 2000; Iizuka *et al*., 2009; Reimink *et al*., 2016; Bauer *et al*., 2017; Reimink *et al*., 2019; Roth *et al*., 2014). Combined with the change in melting depth, these observations indicate a fundamental shift in the processes of TTG production at ~3.6 Ga in this region. The input of relatively juvenile material ~3.6 Ga in the AGC, which is also documented in global zircon Hf isotopic record, shows Hf isotope evidence of interaction with Hadean material. Along with the AGC zircon oxygen isotope record, this requires the input of surface-derived material at depth underneath a pre-existing crustal nucleus.

The source to these 3.75-3.96 Ga rocks was significantly older crust, as indicated by the increasingly negative zircon ε_{Hf} values as well as low whole-rock μ^{142}Nd (Fig. 2 in Reimink *et al*., 2018a). In contrast, the ~3.6 Ga rocks were generated by a mixture of a relatively juvenile source and older evolved crust, with direct assimilation indicated by the presence of >3.7 Ga xenocrystic zircons in 3.6 Ga rocks (Iizuka *et al*., 2006; Reimink *et al*., 2016a). At ~3.6 Ga, variable interaction with the older, pre-existing crustal nucleus is evidenced by the spread in ε_{Hf} (~10 ε_{Hf} units) as well as the existence of older xenocrystic zircons within the ~3.6 Ga magmatic suite (Reimink *et al*., 2016a; Iizuka *et al*., 2007). The combination of the Hf- and O-isotope data are inconsistent with continued thickening of a single Hadean protocrustal block. Rather, the transition in Hf isotope compositions at ~3.6 Ga requires an external, younger source and the O-isotope data an efficient mechanism for the transit of surficial material to great depth. We have proposed that the geochemistry of 4.0 to <3.6 Ga AGC rocks documents a transition from repeated reworking of an ancient, long-lived protocrustal nucleus to a mobile-lid system that transported young, surface-derived crust to depth beneath the nucleus (Reimink *et al*., 2018a).

Statistical and visual evaluation of the regional and global trends

We have applied several statistical and visualisation approaches to test the temporal changes in Hf isotope composition inferred from the global Hadean and early Archean zircon record. We present the data as stacked probability density estimates, and then evaluate the binned age statistics and the change point analysis of the mean values of these datasets with time. These are discussed in detail below.

First, to evaluate changes in ε_{Hf} values with time, we have taken regional and global data sets and subdivided them into 50 Myr age bins. The ε_{Hf} values (without uncertainties) were then plotted as a probability density estimator using the geom_density_ridges density estimator in the R software program (package: ggplot2). This approach can identify age intervals with distinct changes in ε_{Hf} distributions, and in particular highlight distribution changes that may be missed when considering a moving mean. For instance, Figure S-1 shows density estimators from each 50 Myr age bin for the Slave craton dataset. Note that the heights of each density curve are normalised to have the same area under each curve. Therefore, sharp peaks in the probability distribution are likely due to small numbers of data in a particular region. The colours under each curve correspond to the number of data points in each age bin.

The trend of decreasing εHf values with decreasing age can readily be seen in the 4.0–3.7 Ga age interval and a bimodal εHf distribution appears at ~ 3.6 Ga. These trends match the distribution of data in the age-ε_{Hf} plot for the Slave craton and show the utility of using stacked distribution plots for datasets that are over plotted (*i.e*., crowded) in X-Y space, such as the global compilation of age-ε_{Hf} data.

In Figure S-2 we show stacked probability density estimators for all individual detrital datasets, along with the global compilation. Though several of the datasets (*e.g*., Singhbhum, Rae, Limpopo) have only a few data points in the oldest population of zircons, the global compilation robustly documents the transition from the progressively lower ε_{Hf} trend to more juvenile ε_{Hf} values in the 3.8–3.6 Ga interval. The bimodal distributions of ε_{Hf} data in the 3.8–3.6 Ga interval show the arrival of a juvenile source into Earth's felsic crustal system, and the diminishing presence of Hadean crustal sources.

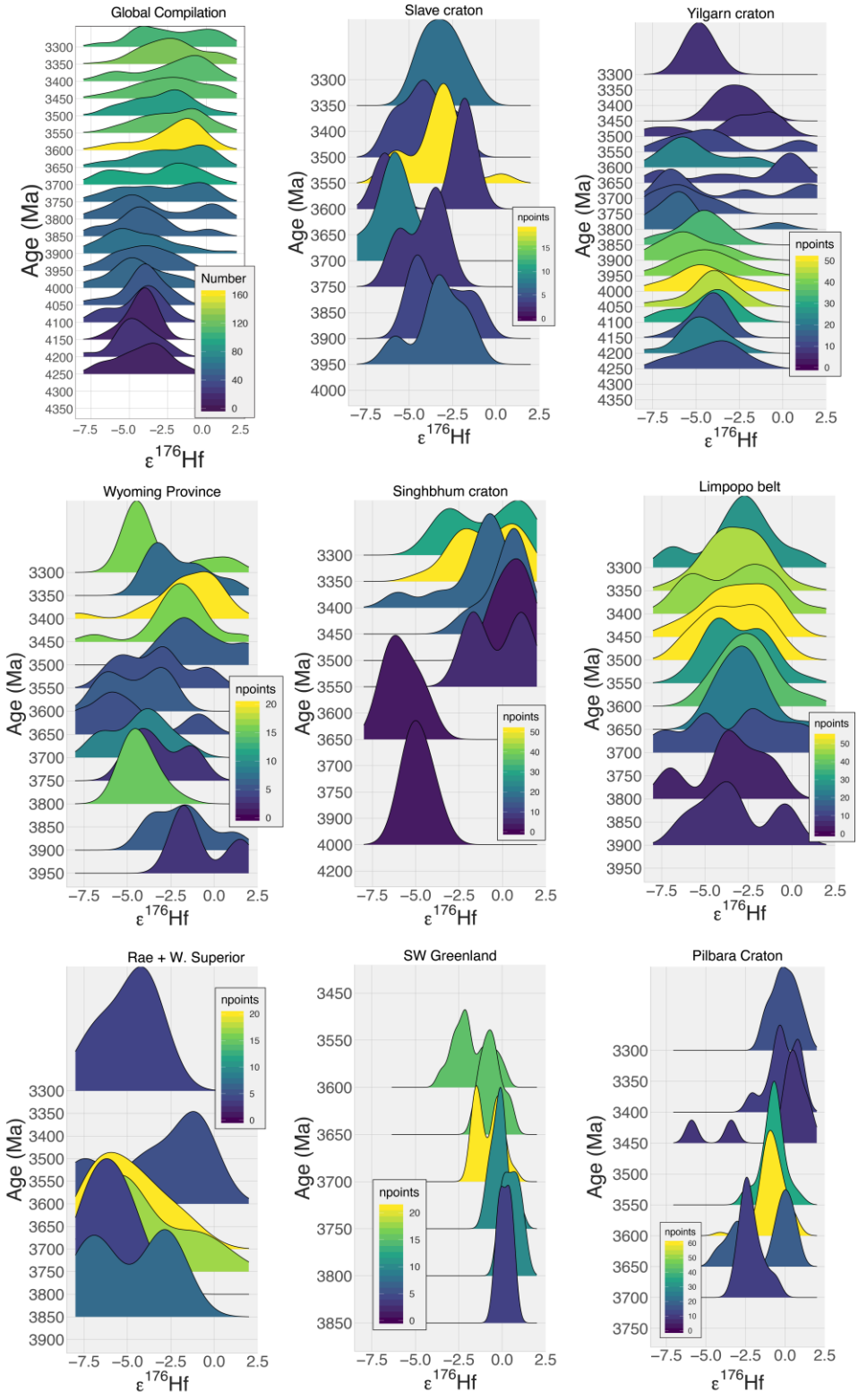

Figure S-2 Stacked probability density plots showing zircon ε_{Hf} values binned in 50 Ma age intervals. Location labels correspond to the plots beneath them and the bandwidth is chosen automatically for the probability densities, which applies to each density curve in an individual plot.

Binned age statistics

A common way to evaluate changes in a time-series analysis is to look at changes in the mean and standard deviations of samples through time. Using the same age bins (50 Myr) and the global compilation dataset, we can see changes in the mean ε_{Hf} value within each age bin. Note, however, that changes in the mean will be naturally subdued and mean values will not be representative of an actual source composition, particularly in the presence of bimodal distributions. This is particularly true in the 3.8–3.6 Ga interval, where the global compilation has a bimodal distribution (Fig. 2).

In Fig. S-3a, the mean ε_{Hf} from each age bin is plotted, with the blue error envelope representing the two standard errors about the mean. An increase in mean ε_{Hf} values begins at ~3.8 Ga, with the mean gradually shifting to higher ε_{Hf} values over the next ~500 Myr. In Fig. S-3b, the standard deviation of each age bin is plotted against age. A step increase in the standard deviation occurs, this time in the 3.9-3.7 Ga age interval. This is an expected result if another source, with a different Hf-isotope composition, is introduced into the system. This observation is not, in and of itself, diagnostic of a new source, as the standard deviation of the global Hf-isotope system is expected to increase over time simply as various reservoirs have more time to evolve to more extreme values, generating a larger spread in ε_{Hf}. However, the correspondence of this increase with the increase in mean ε_{Hf} value, with the arrival of a new source shown by bimodality in ε_{Hf} distributions in Fig. S-2, and the threshold analysis, discussed below, is entirely consistent with our analysis.

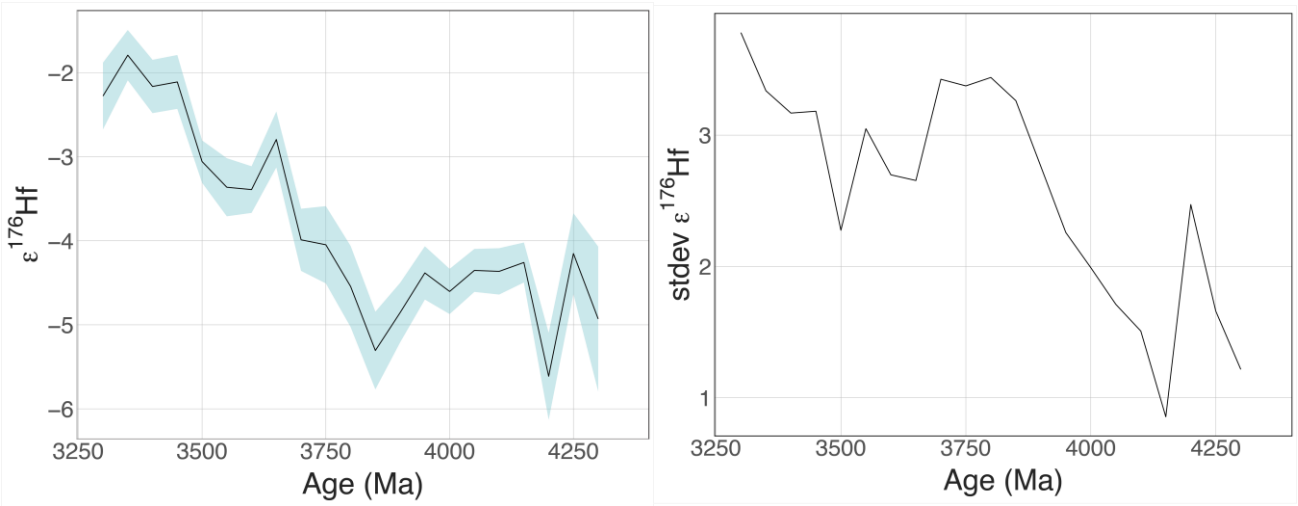

Figure S-3 **(a)** The mean εHf (blue band is 2SE about the mean) at 50 Myr age bins for global detrital and magmatic zircons considered in this study. **(b)** The moving standard deviation of zircon εHf values within each age bin.

Change-point analysis

Change-point analysis is a widely used statistical technique that is commonly employed to search for changes in means or variance of time-resolved data sets. We employ change point analysis, using the chgnpt package in R (Fong *et al*., 2019). This particular implementation of change-point analysis, or more precisely threshold regression analysis, allows for hypothesis testing using several threshold regression models, including the so-called "segmented" threshold effect, which is most applicable to the types of data and underlying processes that we are attempting to evaluate. We chose this strategy as it appears to be the best method for detecting changes in source composition in age-ε_{Hf} data sets, where we are looking for shifts in isotopic composition that reflect large-scale changes in the source to the zircons and their parental magmas, be it older crustal material or a depleted mantle component. Therefore, we are attempting to discern changes in the slope of an underlying fit line which can represent the source to felsic rocks through time and its evolution in Hf-isotope space. Note, however, that a fit line may not always represent a real reservoir that is evolving along a Lu/Hf trajectory but may instead represent a systematic change in the mean due to the input from a new source. For instance, while we interpret the slope of a regression line through the oldest Slave craton data (Fig. S-4) to represent a real reservoir evolving towards negative ε_{Hf} (low Lu/Hf reservoir), the slope of the next trajectory line, after the threshold change, is not representative of a real source as it would require a highly depleted mantle that evolved from a low ε_{Hf} value at 3.6 Ga, an unlikely process.

Using the example of the Slave craton data, we can see the outputs from the threshold regression analysis. The first panel shows the input age-ε_{Hf} dataset for the Slave craton (data sources discussed in previous sections). The red line is the regression corresponding to the threshold change indicated by the threshold regression model. The second panel shows the likelihood of change from the restricted regression models with fixed change points, with real data points plotted as well. The bottom panel shows a histogram of the frequency of threshold estimates in a bootstrapped model of the existing dataset. Notably, this threshold regression analysis indicates that a significant change in the mean ε_{Hf} of the Slave craton data occurred in the 3.7-3.75 Ga interval. This agrees with our interpretation that the 3.6 Ga event in the Slave represents the arrival of a new, more juvenile, source to magmatism in the AGC (*e.g.*, Reimink *et al.*, 2018a and references therein).

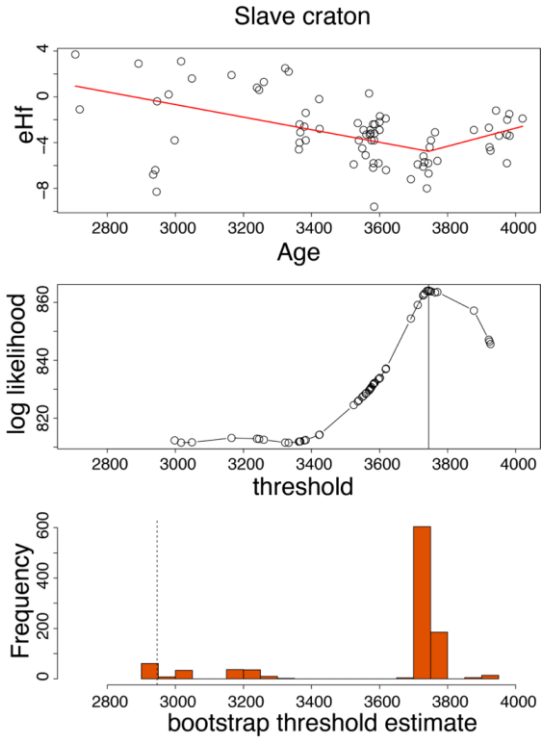

Figure S-4 Changepoint analysis for the Slave Craton.

Global compilation

The threshold regression model suggests a major change at 3.8-3.9 Ga in the global compilation of zircon ε_{Hf}. This change appears to be significantly older than the change at ~3.6 Ga documented in the Slave craton and other regions. However, as discussed in the main text, grouping all regions in one, global, analysis will necessarily 'smear out' any transition that does not occur at precisely the same time. For example, the earliest of two transitions toward higher ε_{Hf} values within the Yilgarn craton occurs near 3.85 Ga (Figs. S-7, S-10), while it occurs in the Slave ~3.6 Ga. An analysis of the combined datasets will be biased towards the dataset with more analyses, in this case the Yilgarn craton which hosts the Jack Hills zircons.

Additional 'smearing' of any transition will be caused by variability in mantle extraction ages of different regions. Again, we can look to the Yilgarn and Slave datasets, where the oldest components of the Slave have chondritic model ages ~4.2 Ga, whereas in the Jack Hills, the chondritic model ages are closer to 4.4 Ga. Combining these two regions will provide a mixed population, and smear any clear change point analysis results. Nevertheless, even when combining all regions to produce a global, but mixed, dataset, threshold regression models indicate a systematic change in zircon ε_{Hf} values in the 3.7-4.0 Ga interval.

In the following plots (Figs. S-5 through S-12), each location is evaluated using the same threshold regression analysis. Some cratons (Wyoming, Yilgarn) have threshold regression results very similar to the Slave craton and the global compilation, while others (Singhbhum, Rae, Limpopo) do not show the same clear transitions. The lack of transitions detected by the threshold regression analysis could be caused by many factors including, limited data in the age interval of interest (Rae), more prominent

transitions at younger ages (Singhbhum), or denser data populations at younger ages (Limpopo). Note that in the case of the Singhbhum craton, a clear trend nearly identical to the Slave craton is seen when the threshold analysis is applied only to analyses >3.4 Ga.

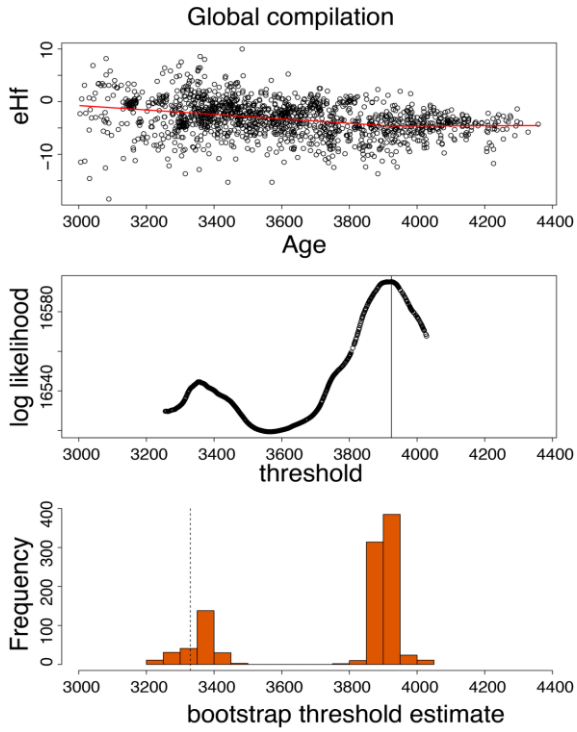

Figure S-5 Changepoint analysis of the global zircon age-ε_{Hf} data compilation.

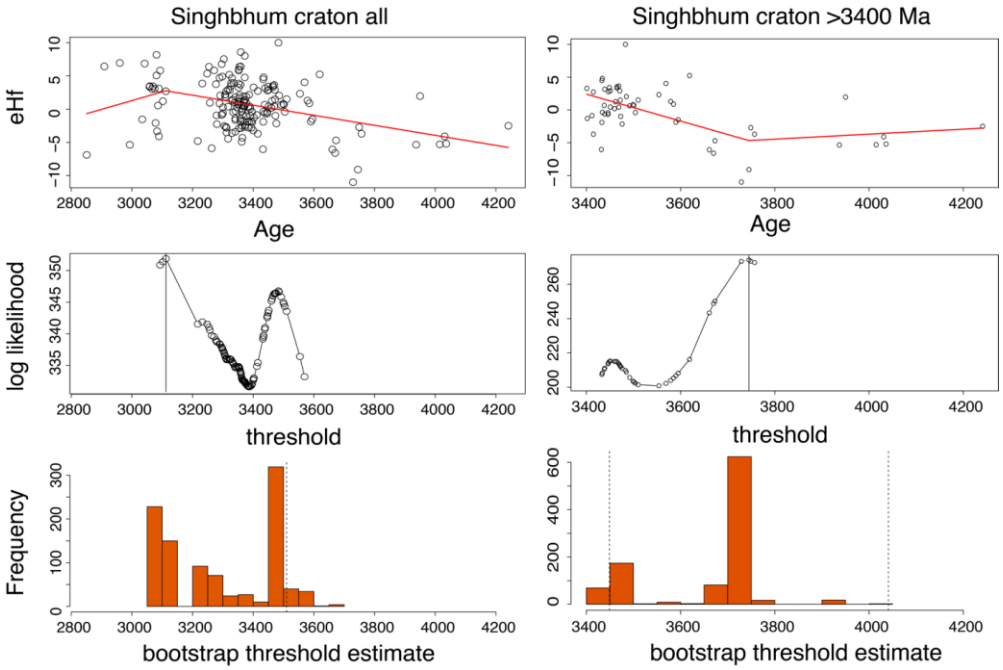

Figure S-6 Changepoint analysis of the Singhbhum craton (at left: all timepoints; at right: >3400 Ma).

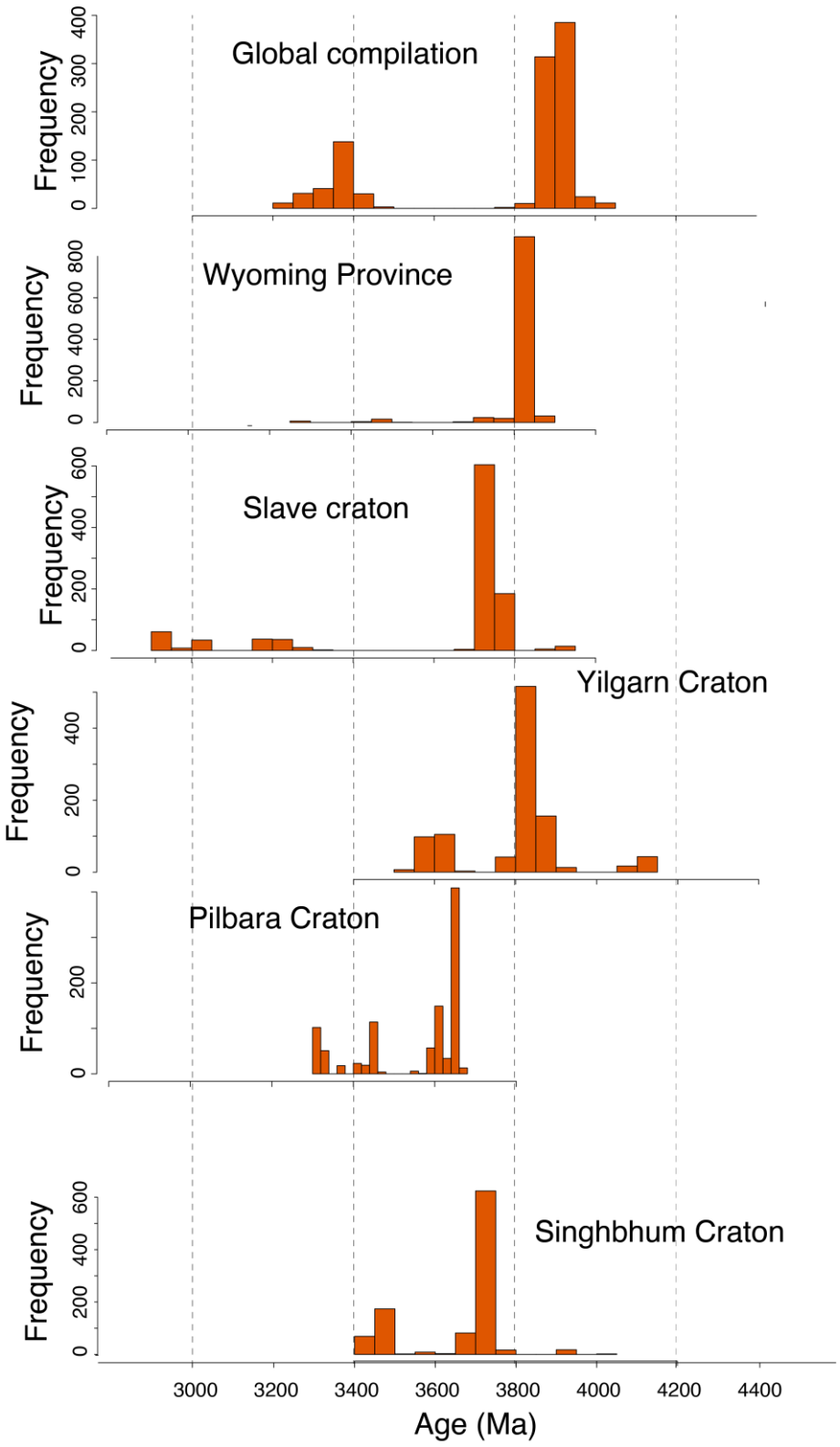

Figure S-7 Compilation of bootstrapped threshold estimates from the changepoint results for several cratons.

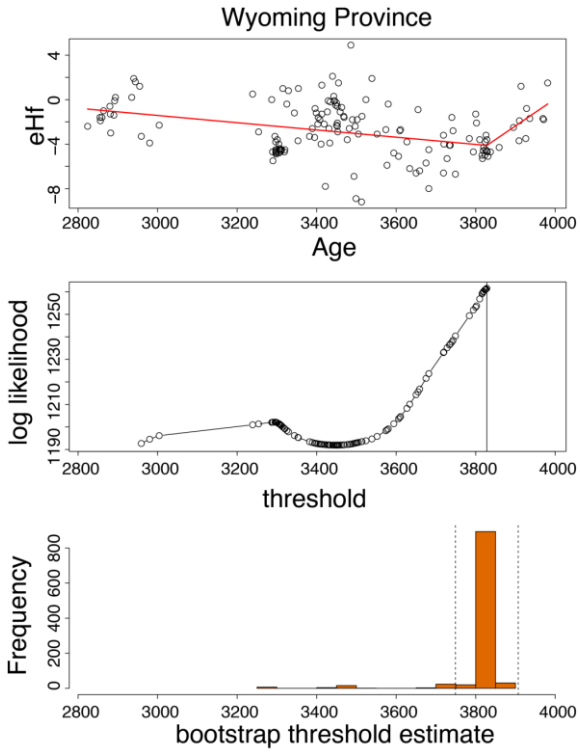

Figure S-8 Changepoint analysis of the Wyoming Province zircons.

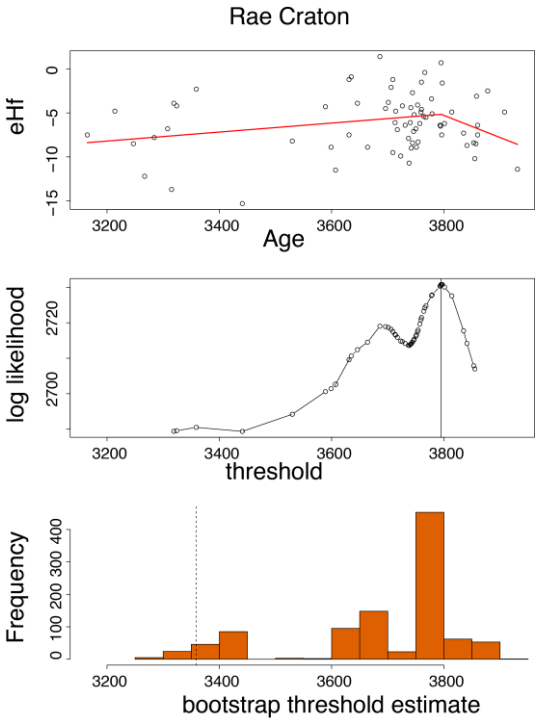

Figure S-9 Changepoint analysis for the Rae Craton and Western Superior Craton zircons.

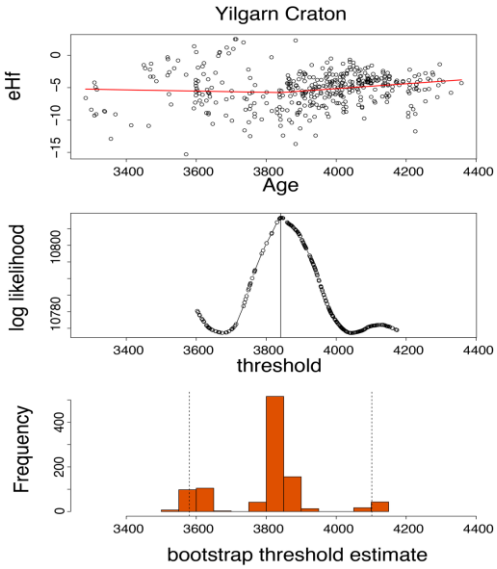

Figure S-10 Changepoint analysis for the Yilgarn craton zircons.

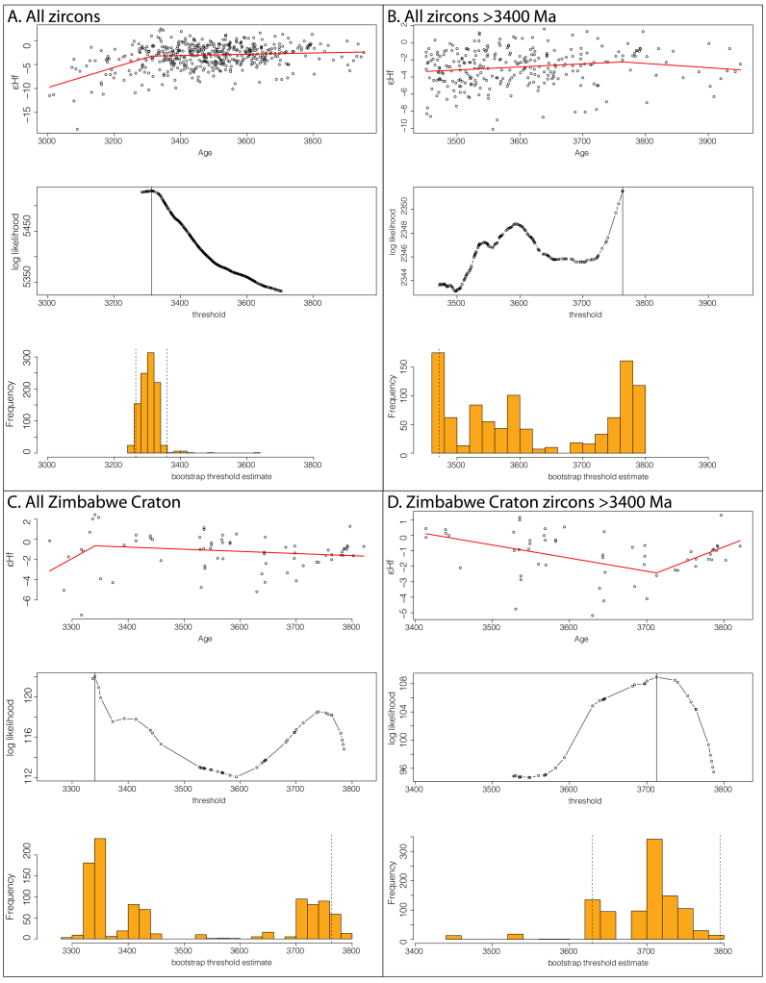

Figure S-11 Changepoint analysis for the combined Limpopo Belt (Zeh *et al.*, 2014) and Zimbabwe Craton (Bolhar *et al.*, 2017) detrital zircons, which may have had a related source. Panel A shows the changepoint analyses for the full dataset, which is dominated by low ε_{Hf} zircons <3200 Ma. Panel B shows the >3.4 Ga subset of all analyses. Panel C shows only those analyses from the Zimbabwe Craton, and a major peak in changepoint likelihood at ~3750 Ma, though not the dominant changepoint. Panel D shows the oldest (>3400 Ma) subset of the Zimbabwe Craton zircons, with a distinct changepoint similar to the Slave craton datasets.

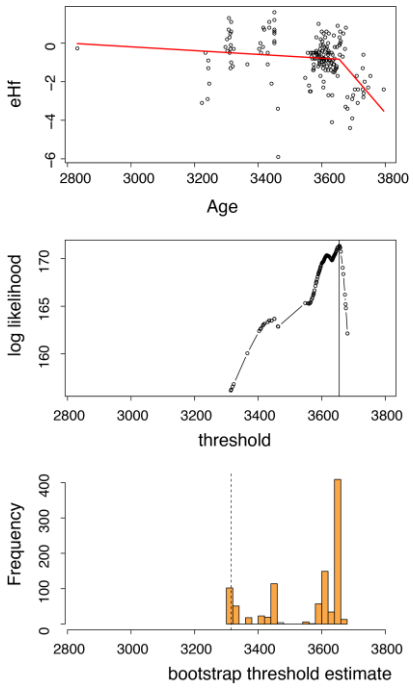

Figure S-12 Changepoint analysis for the Pilbara craton zircons.

Other Archean detrital and metaigneous zircon datasets

The similarity of Hf-isotope trends between the AGC and the Hadean–Eoarchean detrital zircon record makes a compelling case that the processes recorded in the AGC during this time were operating at a global scale. Here we compare the AGC zircon Hf isotope record with three additional terranes. The North Atlantic Craton zircon Hf isotope record is consistent with juvenile compositions from 3.9-3.7 Ga, similar to the evolution of the SW Greenland and the Nuvvuagittuq greenstone belts. There is also limited zircon ε_{Hf} data from the Ancient Gneiss Complex, southern Africa. These rocks do not appear to contain Hadean material and the oldest rocks (~3.66 Ga) have negative ε_{Hf} values, consistent with remelting or assimilation of older (but likely not Hadean) material. At ~3.5 Ga, there is input of relatively juvenile material, corresponding to a diminution of isotopic signals of the oldest crustal materials in this region in the <3.5 Ga magmatic generations. Notably, neither of these terrains contain identified >3.9 Ga zircon material and compare well with locations such as SW Greenland. They may simply not preserve a heritage of stagnant-lid crust production and instead only record felsic crust production at the onset of juvenile growth in a plate-margin setting.

We would also like to acknowledge here that the similarities between the Acasta Gneiss Complex ε_{Hf}-time trends and those of the Rae and W.Superior cratons and Limpopo Belt are more difficult to evaluate (the statistical change point analysis of these cratons is presented in S-9 and S-11). An important point, however, is that the Rae and West Superior regions have very few data. The Limpopo Belt dataset has significant scatter in each age interval, however, when Zeh *et al* (2014) used oxygen isotopes and CL imaging to filter the dataset, the remaining number of analyses is prohibitively small. It is therefore our opinion that these terranes must be further analysed in detail, and our manuscript provides a testable model to motivate this future work.

Methods

Zircon Hf-isotope data were compiled from the following references, divided by location. All initial ε_{Hf} values were calculated using the 176Lu decay constant of Scherer *et al* (2001) and the CHUR Lu-Hf parameters of Bouvier *et al* (2008).

The Acasta Gneiss Complex data plotted here is taken from Reimink *et al*. (2016a), Amelin *et al*. (1999), Iizuka *et al* (2009), Reimink *et al*., (2016b), Bauer *et al*. (2017), Reimink *et al*. (2019), Amelin *et al*. (2000), Iizuka and Hirata (2005), and the subset of zircon data from Guitreau *et al* (2012) which matches the corresponding whole rock Hf isotope systematics. Sample SAB-96-55 of the Acasta Gneiss Complex dataset of Bauer *et al*. (2017) was excluded from the figures in this paper because subsequent zircon U-Pb analysis has revealed further complexity in the age interpretation and assignment. The Central Slave Basement Complex data

comes from Reimink *et al* (2019), and the detrital Slave data from Pietranik *et al* (2008).

The Jack Hills and Narryer Gneiss Terrane dataset includes detrital zircons from the Jack Hills (Amelin *et al*., 1999; Kemp *et al*., 2010; Amelin *et al*., 2000; Bell *et al*., 2014; Harrison *et al*., 2008) as well as metaigneous zircons from the Narryer gneisses (Kemp *et al*., 2010).

Some of the zircon Hf isotope results from the Nuvvuagittuq Greenstone Belt of northern Quebec (O'Neil *et al*., 2013) are plotted as modes of Hf isotope composition instead of weighted means, as presented in the original publication. The uncertainty bars on those samples represent the range in measurements and do not represent the analytical uncertainty. The remaining data are from Augland *et al*. (2015).

Zircons from SW Greenland are from orthogneisses (Amelin *et al*., 2000 and 2011; Fisher and Vervoort, 2018; Hiess *et al*., 2009 and 2011; Kemp *et al*., 2009; Næraa *et al*., 2012), felsic volcanics (Hiess *et al*., 2011; Kemp *et al*., 2009), and metasediments (Næraa *et al*., 2012). The uncertainties presented for the results of Amelin *et al*. (2000) are the 2SD of the weighted means. The age interpretations in Fisher and Vervoort (2018) are in part from Bennett *et al* (1993) and Nutman *et al*. (2000) and unpublished data from G.E. Gehrels.

U-Pb and Lu-Hf isotope signatures of detrital zircons from a quartzite from the Rae Craton and a metagraywacke from the Assean Lake area, NW Superior Province, are from Hartlaub *et al* (2006).

Zircon ε_{Hf} signatures from detrital zircons of the Wyoming craton are from quartz-rich metasediments of the Beartooth Mountains, Wyoming (Mueller and Wooden, 2012) and magmatic zircons from orthogneisses of the Sacawee Block of the Granite Mountains, Wyoming (Frost *et al*., 2017). The results from (Frost *et al*., 2017) are plotted at the measured zircon U-Pb ages in correspondence with how they were presented in that publication; the uncertainties have not been plotted but the 2σ vary between 6 and >100, with a typical value of ~20 Myr.

Magmatic zircons from the Singhbhum craton are from granitoids (Dey *et al*., 2017), the Older Metamorphic Tonalitic Gneiss and Paloearchean TTGs (Chaudhuri *et al*., 2018). Detrital zircons are from a modern river sediment (Miller *et al*., 2018). Detrital zircons from quartzites of the Limpopo Belt are from Zeh *et al*. (2014). The xenocrystic zircons from the Pilbara craton are from Petersson *et al* (2019) and other datasets compiled in that work.

Supplementary Information References

Amelin, Y., Lee, D.C., Halliday, A.N. (2000) Early-middle Archaean crustal evolution deduced from Lu-Hf and U-Pb isotopic studies of single zircon grains. *Geochimica et Cosmochimica Acta* 64, 4205–4225.

Amelin, Y., Kamo, S.L., Lee, D.-C. (2011) Evolution of early crust in chondritic or non-chondritic Earth inferred from U–Pb and Lu–Hf data for chemically abraded zircon from the Itsaq Gneiss Complex, West Greenland. *Canadian Journal of Earth Science* 48, 141–160.

Augland, L.E., David, J. (2015) Protocrustal evolution of the Nuvvuagittuq Supracrustal Belt as determined by high precision zircon Lu–Hf and U–Pb isotope data. *Earth and Planetary Science Letters* 428, 162–171.

Bell, E.A., Harrison, T.M., Kohl, I.E., Young, E.D. (2014) Eoarchean crustal evolution of the Jack Hills zircon source and loss of Hadean crust. *Geochimica et Cosmochimica Acta* 146, 27–42.

Bennett, V.C., Nutman, A.P., McCulloch, M.T. (1993) Nd isotopic evidence for transient, highly depleted mantle reservoirs in the early history of the Earth. *Earth and Planetary Science Letters* 119(3), 299-317.

Bleeker, W., Ketchum, J.W., Jackson, V.A., Villeneuve, M.E. (1999) The Central Slave Basement Complex, Part I: its structural topology and autochthonous cover. *Canadian Journal of Earth Science* 36, 1083–1109.

Bouvier, A., Vervoort, J.D. Patchett, P.J. (2008) The Lu–Hf and Sm–Nd isotopic composition of CHUR: Constraints from unequilibrated chondrites and implications for the bulk composition of terrestrial planets. *Earth and Planetary Science Letters* 273, 48–57.

Chaudhuri, T., Wan, Y., Mazumder, R., Ma, M., Liu, D. (2018) Evidence of Enriched, Hadean Mantle Reservoir from 4.2-4.0 Ga zircon xenocrysts from Paleoarchean TTGs of the Singhbhum Craton, Eastern India. *Scientific Reports* 8, 1-12.

Dey, S., Topno, A., Liu, Y., Zong, K. (2017) Generation and evolution of Palaeoarchaean continental crust in the central part of the Singhbhum craton, eastern India. *Precambrian Research* 298, 268–291.

Fisher, C.M., Vervoort, J.D. (2018) Using the magmatic record to constrain the growth of continental crust—The Eoarchean zircon Hf record of Greenland. *Earth and Planetary Science Letters* 488, 79–91.

Flament, N., Coltice, N., Rey, P.F. (2008) A case for late-Archaean continental emergence from thermal evolution models and hypsometry. *Earth and Planetary Science Letters* 275, 326–336.

Fong, Y. (2019) Fast Bootstrap Confidence Intervals for Continuous Threshold Linear Regression. *Journal of Computational and Graphical Statistics* 28(2), 466-470.

Frost, C.D., McLaughlin, J.F., Frost, B.R., Fanning, C.M., Swapp, S.M., Kruckenberg, S.C., Gonzalez, J. (2017) Hadean origins of Paleoarchean continental crust in the central Wyoming Province. *Geological Society of America Bulletin* 129, 259-280.

Froude, D.O., Ireland, T.R., Kinny, P.D., Williams, I.S., Compston, W., Williams, I.R., Myers, J.S. (1983) Ion microprobe identification of 4,100–4,200 Myr-old terrestrial zircons. *Nature* 304, 616–618.

Guitreau, M., Blichert-Toft, J., Martin, H., Mojzsis, S.J. (2012) Hafnium isotope evidence from Archean granitic rocks for deep-mantle origin of continental crust. *Earth and Planetary Science Letters* 337-338, 211–223.

Harrison, T.M., Schmitt, A.K., McCulloch, M.T., Lovera, O.M. (2008) Early (≥ 4.5 Ga) formation of terrestrial crust: Lu-Hf, $\delta^{18}O$, and Ti thermometry results for Hadean

zircons. *Earth and Planetary Science Letters* 268, 476–486.

Hartlaub, R.P., Heaman, L.M., Simonetti, A., Böhm, C.O. (2006) Relicts of Earth's earliest crust: U-Pb, Lu-Hf, and morphological characteristics of> 3.7 Ga detrital zircon of the western Canadian Shield. *Geological Society of America Special Papers* 405, 75–89.

Hiess, J., Bennett, V.C., Nutman, A.P., Williams, I.S. (2009) In situ U–Pb, O and Hf isotopic compositions of zircon and olivine from Eoarchaean rocks, West Greenland: New insights to making old crust. *Geochimica et Cosmochimica Acta* 73, 4489–4516.

Hiess, J., Bennett, V.C., Nutman, A.P., Williams, I.S. (2011) Archaean fluid-assisted crustal cannibalism recorded by low δ18O and negative εHf(T) isotopic signatures of West Greenland granite zircon. *Contributions to Mineralogy and Petrology* 161, 1027–1050.

Iizuka, T., Hirata, T. (2005) Improvements of precision and accuracy in in situ Hf isotope microanalysis of zircon using the laser ablation-MC-ICPMS technique. *Chemical Geology* 220, 121–137.

Iizuka, T., Horie, K., Komiya, T., Maruyama, S., Hirata, T., Hidaka, H., Windley, B.F. (2006) 4.2 Ga zircon xenocryst in an Acasta gneiss from northwestern Canada: Evidence for early continental crust. *Geology* 34, 245–248.

Iizuka, T., Komiya, T., Ueno, Y., Katayama, I., Uehara, Y., Maruyama, S., Hirata, T., Johnson, S.P., Dunkley, D.J. (2007) Geology and zircon geochronology of the Acasta Gneiss Complex, northwestern Canada: New constraints on its tectonothermal history. *Precambrian Research* 153, 179–208.

Kemp, A.I.S., Foster, G.L., Schersten, A., Whitehouse, M.J., Darling, J., Storey, C. (2009) Concurrent Pb–Hf isotope analysis of zircon by laser ablation multi-collector ICP-MS, with implications for the crustal evolution of Greenland and the Himalayas. *Chemical Geology* 261, 244–260.

Ketchum, J., Bleeker, W., Stern, R.A. (2004) Evolution of an Archean basement complex and its autochthonous cover, southern Slave Province, Canada. *Precambrian Research* 135, 149–176.

Miller, S.R., Mueller, P.A., Meert, J.G., Kamenov, G.D., Pivarunas, A.F., Sinha, A.K., Pandit, M.K. (2018) Detrital zircons reveal evidence of Hadean crust in the Singhbhum Craton, India. *The Journal of Geology* 126, 541–552.

Næraa, T., Schersten, A., Rosing, M.T., Kemp, A.I.S., Hoffman, J.E., Kokfelt, T.F., Whitehouse, M.J. (2012) Hafnium isotope evidence for a transition in the dynamics of continental growth 3.2 Gyr ago. *Nature* 485, 627–630.

Nutman, A., Bennett, V.C., Friend, C., McGregor, V. (2000) The early Archaean Itsaq Gneiss Complex of southern West Greenland: the importance of geology in interpreting geochronological and isotopic data for early terrestrial evolution. *Geochimica et Cosmochimica Acta* 64, 3035-3060.

Mueller, P.A., Wooden, P.A. (2012) Trace Element and Lu-Hf Systematics in Hadean-Archean Detrital Zircons: Implications for Crustal Evolution. *The Journal of Geology* 120, 15–29.

Petersson, A., Kemp, A. I., & Whitehouse, M. J. (2019) A Yilgarn seed to the Pilbara Craton (Australia)? Evidence from inherited zircons. *Geology* 47(11), 1098-1102.

Pietranik, A.B., Hawkesworth, C.J., Storey, C.D., Kemp, A.I.S., Sircombe, K.N., Whitehouse, M.J., Bleeker, W. (2008) Episodic, mafic crust formation from 4.5 to 2.8 Ga: New evidence from detrital zircons, Slave craton, Canada. *Geology* 36, 875–878.

Reimink, J.R., Davies, J.H.F.L., Chacko, T., Stern, R.A., Heaman, L.M., Sarkar, C., Schaltegger, U., Creaser, R.A., Pearson, D.G. (2016) No evidence for Hadean continental crust within Earth's oldest evolved rock unit. *Nature Geoscience* 9, 777-780.

Roth, A.S.G., Bourdon, B., Mojzsis, S.J., Rudge, J.F., Guitreau, M., Blichert-Toft, J. (2014) Combined ^{147,146}Sm- ^{143,142}Nd constraints on the longevity and residence time of early terrestrial crust. *Geochemistry Geophysics Geosystems* 15, 2329–2345.

Scherer, E.E., Münker, C., Mezger, K. (2001) Calibration of the Lutetium-Hafnium Clock. *Science* 293, 683–687.

Thern, E.R., Nelson, D.R. (2012). Detrital zircon age structure within ca. 3Ga metasedimentary rocks, Yilgarn Craton: Elucidation of Hadean source terranes by principal component analysis. *Precambrian Research* 214-215, 28–43.

Zeh, A., Stern, R. A., Gerdes, A. (2014) The oldest zircons of Africa—Their U–Pb–Hf–O isotope and trace element systematics, and implications for Hadean to Archean crust–mantle evolution. *Precambrian Research* 241, 203–230.